1-1-2015

Dependence of texture development on the grain size of tertiary oxide scales formed on a microalloyed steel

Xianglong Yu
University of Wollongong, xly991@uowmail.edu.au

Zhengyi Jiang
University of Wollongong, jiang@uow.edu.au

Jingwei Zhao
University of Wollongong, jzhao@uow.edu.au

Dongbin Wei
University of Wollongong, dwei@uow.edu.au

Ji Zhou
Tsinghua University

See next page for additional authors

Dependence of texture development on the grain size of tertiary oxide scales formed on a microalloyed steel

Abstract

Both orientational and geometrical characteristics of grains in tertiary oxide scales have been quantitatively investigated using the electron backscatter diffraction (EBSD) technique. Phase and orientation mappings demonstrate that the {001} planes of magnetite and the {0001} planes of hematite are parallel to the direction of oxide growth. Pole figures (PFs) as scattering plots clearly display the direct correlation between the orientations and microstructure sites of magnetite grains. Magnetite grains develop a strong rotated cube texture component that shifts to the {100} component, whereas those with the grain size of 1-5. μm develop the {001} cube texture component. The refined magnetite grains surrounding the abnormal ones can be a combined process, including magnetite pro-eutectoid during hot rolling and cooling and re-oxidation during air-cooling. Our findings offer insights toward further understanding of the link between the geometrical and orientation parameters of grains with respect to the deformation behaviour of oxide scales formed at elevated temperatures.

Keywords

scales, formed, microalloyed, steel, development, grain, size, tertiary, texture, oxide, dependence

Disciplines

Engineering | Science and Technology Studies

Publication Details

Yu, X., Jiang, Z., Zhao, J., Wei, D., Zhou, J., Zhou, C. & Huang, Q. (2015). Dependence of texture development on the grain size of tertiary oxide scales formed on a microalloyed steel. Surface and Coatings Technology, 272 39-49.

Authors

Xianglong Yu, Zhengyi Jiang, Jingwei Zhao, Dongbin Wei, Ji Zhou, Cunlong Zhou, and Qingxue Huang

Dependence of texture development on the grain size of tertiary oxide scales formed on a microalloyed steel

Xianglong Yu [1, 2], Zhengyi Jiang [1, 4*], Jingwei Zhao [1], Dongbin Wei [1, 3], Ji Zhou [2], Cunlong Zhou [4 *], Qingxue Huang [4]

[1] School of Mechanical, Materials and Mechatronic Engineering, University of Wollongong, Wollongong, NSW 2522, Australia

[2] School of Materials Science and Engineering, Tsinghua University, Beijing 100084, China

[3] School of Electrical, Mechanical and Mechatronic Systems, University of Technology, Sydney, NSW 2007, Australia

[4] Shanxi Provincial Key Laboratory on Metallurgical Device Design and Theory, Taiyuan University of Science and Technology, Shanxi 030024, China

Abstract

Both orientational and geometrical characteristics of grains in tertiary oxide scales have been quantitatively investigated using the electron backscatter diffraction (EBSD) technique. Phase and orientation mappings demonstrate that the {001} planes of magnetite and the {0001} planes of hematite are parallel to the direction of oxide growth. Pole figures (PFs) as scattering plots clearly display the direct correlation between the orientations and microstructure sites of magnetite grains. Magnetite grains develop a strong rotated cube texture component that shifts to the {100}<210> component, whereas those with the grain size of 1-5 μm develop the {001}<100> cube texture component. The refined magnetite grains surrounding the abnormal ones can be a combined process, including magnetite pro-eutectoid during hot rolling and cooling and re-oxidation during air-cooling. Our findings offer insights toward further understanding of the link between the geometrical and orientation parameters of grains with respect to the deformation behaviour of oxide scales formed at elevated temperatures.

Keywords: Grain size; Orientation; EBSD; Oxide scale; Microalloyed steel.

*Corresponding authors: Tel: 61 2 42214545; Fax: 61 2 42215474; Email: jiang@uow.edu.au (Z.Y. Jiang). Tel: 86 18635592059; Fax: 86 351 6963332; Email: zcunlong@163.com (C. Zhou).

1. Introduction

Most metals and alloys inevitably form surface oxide layers due to rapid oxidation during processing at high temperatures, generally at 500 °C and above [1]. Consequently, the formed metallic oxides (scales) have posed a serious obstacle to ensuring a defect-free surface of the steel product in an ecologically friendly way [2, 3]. With this in mind, the nature of the surface layers produced on the metal plays a major role in the behaviour of the materials, particularly when exposed to high temperatures and oxidising atmospheres [4, 5]. In the case of hot rolling, the surface properties include the surface energy, crystallographic orientation, grain boundaries, texturing of the surface and crystal structure [6]. It is therefore widely expected that tailoring the atomic structure of the oxide layers can enhance tribological properties during environmentally friendly nanoparticle lubrication and further improve the surface quality of the final products [7]. However, the evaluation of individual grain features, such as grain size and orientation, in oxide layers has received less investigation.

In the particular case of hot rolling, oxide scales can generally be classified as primary, secondary and tertiary oxide scales. The three types of oxide scales normally correspond to the reheating stages, the roughing stages and the finishing passes of continuous mills, respectively [8]. As the final produced on the hot-rolled steel strip, the tertiary oxide scale grows during the finishing rolling and the subsequent cooling down to ambient temperature. The oxide scale is therefore deformed while the steel is processed [9]. In most cases, the tertiary oxide scale consists of a thin outer layer of hematite (α-Fe_2O_3), an intermediate layer of magnetite (Fe_3O_4), and an inner layer of wustite ($Fe_{1-x}O$, with 1-x ranging from 0.83 to 0.95) just above the steel substrate [2, 8, 9]. These layers of oxide scales may evolve further and undergo structural changes if oxygen is available during air-cooling after coiling [7, 8]. Hence, the distribution of these oxide phases depends largely on the

heat treatment and atmospheric conditions during hot rolling and the alloying elements contained in the steel compositions [8, 10]. In particular, phase distributions within oxide scales will be elusive when considering wustite decomposition below 570 °C and re-oxidation of magnetite in open-air storage of hot-coiled steel [11-13]. In addition, it is still unknown how to characterise the crystallographic texture evolution in tertiary oxide layers.

Measurements of grain size and phase identification in oxide scales have previously been performed using optical microscopy with conventional sample preparation [8, 14]. Nevertheless, the main challenge is the complicated and time-consuming polishing procedures because the oxide phases and the steel substrate need to be polished at different rates [15]. Sometimes, one or two phases are still difficult to identify, even after etching in a 0.5-1% hydrochloric acid solution in ethanol [14]. With the electron backscatter diffraction (EBSD) technique combined with ion miller sample preparation, only crystallographic characterisation is relied on to determine a grain rather than etching and others [15]. Automated EBSD has therefore become the ideal technique for concurrent access to both the spatial distribution of the grain size and the crystallographic orientation in oxide scales [16], which in turn permits correlations to be made between the two. Texture measurements can hence also be linked to grain size, such as the effect of second-phase particles on the rate of grain refinement in an aluminium alloy [17]. However, the link between grain size and texture evolution in the tertiary oxide scale formed on hot-rolled steel is still unknown.

In this present study, four cases of different grain sizes and orientation distributions in tertiary oxide scales were analysed using EBSD in an attempt to quantitatively evaluate the corresponding texture evolution. Based on our previous studies [18, 19], what we can gain in the current work is a deeper understanding of the microstructural features and crystallographic texture associated with deformation behaviour of oxide scales formed at elevated temperatures.

2. Experimental and analytical procedures

2.1 Material and HR-AC tests

The material used in this study is a microalloyed low-carbon steel with chemical compositions (wt.%) as follows: C 0.1, Si 0.15, Mn 1.61, Cr 0.21, Al 0.034, P 0.014, S 0.002, N 0.003, Nb + V + Ti 0.016-0.041, and balance Fe. The steel samples were cut into 400 × 100 × 3 mm^3 sheet, ground using SiC papers with 2400 mesh to a surface finish of 0.5 μm, and cleaned in a solution of acetone prior to hot rolling combined with accelerated cooling (HR-AC) tests.

HR-AC experiments were performed on a 2-high Hille 100 experimental mill equipped with an accelerated cooling system. Full details of the experimental instruments can be found elsewhere [20, 21]. The following procedure was carried out for every HR-AC test. Each sheet was reheated to 900 °C at a rate of 1.7 °C/s under a high-purity nitrogen atmosphere, and held for 15 min to ensure a uniform temperature and homogenise the austenite grains. The reheated sheet was then rolled for a thickness reduction of 28% at a rolling speed of 0.3 m/s and a rolling temperature of approximately 860 °C without any lubrication, followed by an accelerated cooling at a rate of 28 °C/s. In this case, the entry/exit temperatures of water-cooling are 784°C and 619 °C, respectively. The latter temperature is similar to the coiling temperature in the conventional hot rolling process [18]. Finally, the hot-rolled sheet was air-cooled to obtain the tertiary oxide scale at room temperature. This assumes that the grown oxide layers are subject to the same deformation ratios as the corresponding hot-rolled steel substrate.

2.2 Analytical methodology

The samples were cut from the centre of the hot-rolled sheet perpendicular to the rolling direction and parallel to the oxide growth in blocks of 20 × 20 × 7.8 mm^3. Hence, the sample surface of oxide growth was oriented in the normal direction (ND). The gauge length and width of the rolling sample were parallel to the rolling direction (RD) and traverse direction (TD) of the hot-rolled strip, respectively. Full details on the procedure to achieve such an oxide scale can be found elsewhere [18, 22].

The sample preparation for electron microscopes was performed on a Leica EM triple ion beam cutter (TIC020) system. After gold deposition, the edges of the sample for cross sectional analysis were ground by SiC papers with 2000 mesh and then ion-milled at 6 kV for 5 h using a TIC020 system. When taken from the mask of the ion miller, the samples were ready for EBSD. Microstructural characterisation was studied using a JEOL JSM 7001F Schottky field emission gun (FEG) scanning electron microscope (SEM) with a Nordlys-II (S) EBSD detector, operated at an acceleration voltage of 15 kV, a probe current of approximately 2–5 nA, a working distance of 15 mm, and a step size of 0.125 µm. The EBSD dataset was acquired and indexed using the Channel 5 software package.

2.3 EBSD analytical procedure

Post-processing of the acquired dataset was also conducted using the Oxford Instruments Channel 5 software package and presented in different ways: using the Tango program for image mapping, Mambo program for the pole figure, and Salsa program for orientation distribution functions (ODFs). All of the EBSD maps were first cleaned by removing wild orientation spikes and filling in

zero solutions via extrapolation up to six neighbours. Any remaining pixelations denoted by negative or zero slopes of the major axis of the fitted equivalent circle ellipsoid were removed based on a shape criterion. A minimum of three pixels is maintained in subgrain structures to remove map artefacts. An angular resolution for the grain reconstruction was maintained at a constant value of 2° to reduce orientation noise and retain orientation contrast/texture information. Accordingly, $2° \leq \theta < 15°$ misorientations are defined as low-angle grain boundaries (LAGBs), whereas the high-angle grain boundaries (HAGBs) are $\theta \geq 15°$. As a consequence, a grain boundary can be classified geometrically in terms of the relative misorientation between the neighbouring grains.

Four subsets with respect to different grain sizes in the oxide sample have been established to analyse the link between grain size and texture evolution; in order of grain size, these subsets are 1-5 μm, 5-10 μm, 10-15 μm and larger than 15 μm. Orientation distributions of the four subsets were calculated from the data on the individual grain orientations collected.

Pole figures are represented by two main methods of density distributions and individual orientations [15], and the resulting plots are continuous contours and scattering data, respectively. Contoured pole figures were obtained on the most prominent crystallographic planes of ferrite and magnetite, (001) and (110), whereas the pole figures as the plot of discrete points provide all crystallographic planes of magnetite.

For ODF representation, the grain orientation $g = (\phi_1, \Phi, \phi_2)$ is expressed by the three Euler angles in Bunge notation [23]. The probability density function of the orientation g can be represented by the ODF in the form of sections through the orientation space. The ODF sections were calculated using the discrete binning method with a bin size of 5º and Gaussian smoothing. Our previous studies [18, 19] have addressed the analytical procedures for such a multiphase oxide scale.

3. Results and discussion

3.1 Phase identification and orientation mapping

Fig. 1 presents the representative phase and inverse pole figure (IPF) maps of the tertiary oxide scale formed on the hot-rolled steel at a thickness reduction of 28% and a cooling rate of 28 °C/s. Both EBSD-derived maps can be compared together to examine the boundary displacement and thereby evaluate the grain reconstruction from a new dataset. The result of the phase analysis in Fig. 1a illustrates the distribution of different oxide phases according to the default colour within a specific scanning map. The phase mapping has a three-layered microstructure, namely a thin layer of hematite, an intermediate layer of magnetite, and the steel substrate. The retained wustite and eutectoid ferrite disperse over the magnetite matrix. Hematite near the surface gradually penetrates into the magnetite, even scattering near the cracking edges in the oxide scale. The distribution of hematite in the oxide scale can be attributed to a lack of crystal continuity when grains of the trigonal hematite grow based on the cubic spinel magnetite. Moreover, previous studies [19, 24] have confirmed that the hematite grains grow tilting at an angle of 60° [24], or a modified value of 54.76° [19], from the <001> crystal direction of magnetite.

As observed in Fig. 1b, the IPF orientation map overlaid with the grain boundary mapping shows the crystallographic orientation of individual grains and the microstructure in the oxide sample. The overlay of the grain boundary map highlights subgrains (2-15°) in light grey and high angle boundaries (> 15°) in shades of black based on the misorientation angle. According to the colour coded for absolute orientations of the individual grains relating to a stereographical triangle, most grains in the top layer of the oxide scale dominate the preferred orientation with {001} in magnetite

or {0001} in hematite parallel to the ND, i.e., along the oxide growth direction. The preferred orientations of grain growth can be determined by the minimisation of surface energy in cubic magnetite [18] and the basal slip in trigonal hematite [19]. Nevertheless, the grains of ferrite in the steel substrate develop almost exclusively preferred orientations described by the {001} texture component. In the case of the surface region of a hot-rolled steel, ferrite would be expected to develop the {011} parallel to the ND or {110} parallel to the TD [25, 26]. This is partly due to the dynamic phase transformation of deformed austenite during hot rolling [15, 27]. In this case, what texture component occurs in the steel substrate will be quantitatively analysed in Section 3.4.

3.2 Characterising grain sizes

The EBSD technique allows for automatic measurement of grain size based on crystallographic characterisation to determine a grain rather than etching or using other traditional methods [14, 16]. The distributions of phases and preferred orientations can hence also be linked to the grain size in the oxide sample. Four cases of different grain sizes and orientation distributions have been analysed to quantitatively describe the link between grain size and texture evolution. In Figs. 2-5, the phase and IPF orientation maps of the oxide sample show the evolution of the microstructure with progressively greater grain sizes.

Compared with the magnetite grains in the other three maps, the grains within the grain size of 1-5 μm in Fig. 2 mainly surround the relatively large grains. Alternatively, the refined grains can grow near the crack initiation of the oxide scale, such as the oxide/substrate interface. During accelerated cooling, the temperatures of the hot-rolled samples were still well above 570 °C, i.e. 619 °C, before air-cooling in this study. The deformed oxide layers during subsequent air-cooling would have undergone further oxidation to magnetite, precipitation of pro-eutectoid magnetite and finally a

eutectoid reaction, forming a mixture of magnetite and ferrite. Then, the grain-refined magnetite near the oxide/substrate interface could form during this time due to the temperature gradient of the oxide scale. The morphology of grains in these two layers is therefore slightly equiaxed. The former of the hematite grains is consistent with the result of the crystal lattice mismatch of hematite and magnetite described in Section 3.1. In the steel substrate, the diameters of ferrite grains are relatively fine (below 10 μm; see Fig. 3) due to the grain refinement of the niobium, vanadium and titanium additions in the microalloyed steel [10, 28]. The relatively coarse grains of magnetite in Fig. 4 suggest the existence of the granular precipitates to a certain extent during the cooling. The phase transformation can be due either to disproportionation or superficial oxidation of wustite in magnetite or both [11-13]. In addition, the grains shift along the rolling direction of the steel sample when the grain size is larger than 15 μm (Fig. 5). This implies that grain-boundary sliding contributes significantly to dissipation in oxide layers during hot rolling.

The preferred orientation of relatively refined grains (Fig. 2b) is, in the presence of the strong texture component {001} parallel to the ND, which is similar to the finding shown in Fig. 1b. This is also the case of the texture evolution dedicated to the grain size dependence of normal anisotropy low-carbon steel strips [29]. The process of grain subdivision in the oxide scale during hot rolling and subsequent cooling is also essential for the formation of ultrafine grains in such an oxide layer. The evolution of the microstructure and texture occurring during the deformation and subsequent annealing can therefore be interpreted as a pronounced recovery process during which new grains are created without a preceding nucleation [30]. The result reveals that the magnetite preferred growth and transformation to occur after the hot rolling. Additionally, it is noted that a cumulative spread of orientation within a grain can be relatively large, as in Fig. 5b, especially for deformed materials. With this in mind, a more subtle consequence of the use of orientation mapping to define

grains is that the specification of a grain in the orientation map is based on the orientation of neighbouring points being within a certain small tolerance of each other [15, 31, 32].

3.3 Pole figure measurements

To quantitatively evaluate the orientation distributions with respect to various ranges of grain sizes, pole figures have been used to display the spherical projection of crystal directions of individual grains in the oxide scale. Four datasets of different grain sizes and orientation distributions, as mentioned in Section 3.2, have been selected to perform the analysis of texture evolutions. In doing so, there are two main methods of representing the orientation data in a pole figure, density distributions and individual orientations [15]. In the case of the two former datasets of the grain sizes of 1-5 μm and 5-10 μm, a continuous density distribution is superior for the representation of larger numbers of orientations with statistical relevance in a pole figure. The resulting contoured pole figures are illustrated in Fig. 6. If the number of orientations is small, such as in Figs. 4b and 5b, the contoured pole figures may look rather unsystematic or 'spiky.' In this case, it might be appropriate to represent the discrete data, as shown in Fig. 7.

In Fig. 6a, the crystallographic texture of the steel substrate, ferrite here, with the grain sizes of 1-5 μm, is weak, holding a maximum texture strength of 4.09. Added to it is evidence that the ferrite grains near the surface of the hot-rolled steel develop nothing of the {001} || ND texture component, as mentioned in Section 3.1. In contrast, magnetite grains with grain sizes of 1-5 μm and 5-10 μm share the similar texture strength, holding a strong {001} fibre component parallel to the ND in Fig. 6b and c. Their maximum values of texture strength are 5.02 and 5.06, respectively. This implies that, for magnetite grains, the polycrystalline substrate requires longer oxidation time [33] or higher deformation to evolve clear {001} fibre textures compared to the iron single crystal [18, 26].

The pole figures in Fig. 7 are displayed as scatter plots to suit the particular case of the relatively large grains limited to a quite small number of individual points. This method is enabled so that local orientation data can be marked in the pole figure with different IPF colour schemes with respect to their location in the microstructure. The orientation of these grains corresponds to Figs. 4b and 5b, respectively, where the IPF orientation maps have several deformed grains in the oxide scale. The orientations are further distinguished as to whether the corresponding grains developed {001} parallel to the ND in the pole figures. Orientations of grains that developed {001} || ND in the oxide scale are marked with the colour red according to the IPF colour scheme with respect to a stereographical triangle. From this, it has been concluded that grain sliding of large magnetite grains is also restricted to some grains with orientations close to the {001} || ND orientation. It is also noted that this does not unequivocally prove that these subgrains actually have the same orientation. This is because the pole figure only shows the orientation of one reference axis, here the oxide growth ND, but rotations about this axis are not considered. For example, the full grain orientations of subgrains in Fig. 5b were quite different, which becomes obvious when plotting the same orientations in a pole figure in Fig. 7b. Therefore, for a complete representation of the 3D orientation information, an ODF representation of texture evolution becomes necessary.

3.4 Orientation distributions of magnetite with various grain sizes

One of the challenges with Euler space and ODF is to recognise common textures. To make this easy, Fig. 8 schematically provides the ideal fibres, including some important texture components, in cubic materials and their positions of ODF distribution for selected sections of fixed ϕ_2 angles [15, 34]. The Euler angles and Miller indices corresponding to these common texture components are listed in Table 1. In most cases, the relevant texture fibres for cubic materials are the α, γ and ε

fibres lying on the ϕ_2 = 45° section at ϕ_1 = 0, Φ = 55°, ϕ_1 = 90°, corresponding to the crystallographic fibre axis around <110> || RD, <111> || ND, and <011> || TD, respectively, and the η, θ and ζ fibres superimposed on the ϕ_2 = 0° section at ϕ_1 = 0, Φ = 0° and Φ = 45°, with the rotations of <100> || RD, <100> || ND and <110> || ND, respectively [15, 26].

The evolutions of the crystallographic texture for magnetite grains in the three subsets are given in Fig. 9. The variation in the intensity $f(g)$ of the individual texture components along the various fibres is illustrated in Fig. 10. The grains of magnetite in the complete map in Fig. 9a contain a strong {001} <110> Rotated Cube (Rt-C) component with the maximum intensity $f(g)$ up to 10. Nevertheless, the relatively strong Rt-C texture component shifting to the {100}<210> component records two equal peaks of texture intensities $f(g)$ = 9.1, as shown in Fig. 10a. For the magnetite with the grain size of 1-5 μm in Fig. 9b, the intensity of the {100}<210> texture component is reduced to $f(g)$ = 6.9 in Fig. 10a. In Fig. 9c, for the grain size of 5-10 μm, a relatively weak θ fibre develops in magnetite, superimposed on the ϕ_2 = 0° section at Φ = 0° with the rotations of <100> || ND, showing its maximum intensity of $f(g)$ = 3.8. This texture evolution shifting from the Rt-C to the {100}<210> texture component has also been found in previous studies [18, 26] using plane strain compression tests. One of the differences is the weak intensity of the {001}<100> cube texture component. In addition to this, magnetite with the grain size of 1-5 μm develops the second maximum intensity $f(g)$ = 3.8, as highlighted in Fig. 10b. This cube texture component is superimposed on the ϕ_2 = 45° section at Φ = 0°. It is also evidence that the preferred orientation of relatively refined grains (Fig. 2b) is, in presence of the strong texture component {001} parallel to the ND, as described in Section 3.1. This can be attributed to the fact that the refined grains grow surrounding the large grains to relieve the deformation during hot rolling, which is also associated with the grain sliding mechanism [35].

3.5 Formation mechanism of the refined magnetite grains

The formation of the refined magnetite grains is a complex process, which could be the combination of pro-eutectoid during hot rolling and cooling and re-oxidation during air-cooling after deformation. Three direct pieces of evidence in this study can account for this. First, based on the temperature ranges and the conventional understanding of oxide scale structure development on low-carbon steel (in this case, the rolling temperature of 860 °C and the entry/exit accelerated cooling temperatures of 784 °C and 619 °C, respectively), the temperature is well above 570 °C, i.e., the temperature of wustite decomposition. Therefore, magnetite can precipitate from the wustite matrix during hot rolling and cooling even though the pro-eutectoid reaction is relatively slow [36]. Second, the high cooling rate of 28 °C/s and the relatively thin thickness of less than 100 μm make the magnetite pro-eutectoid difficult, due mainly to the temperature changes within the oxide scale being relatively uniform. As such, the slow pro-eutectoid reaction is dominant before air-cooling. Finally, compared to previous texture studies [26, 33], the texture evolution of magnetite in Fig. 9 is similar to the findings of the oxides formed on an ultra-low-carbon steel that was reheated for 5 s at 1050 °C and subjected to a 70% reduction in height by plane strain compression [26]. This implies that the {001} fibre of magnetite in Fig. 10a is derived from the re-oxidation of the formed oxide at high temperature, which can also be found elsewhere [24, 33]. Alternatively, the {110} fibre texture of magnetite in Fig. 10b shares a similar source in the magnetite layer after 1 h of oxidation of the iron single crystal below 450°C [33]. The texture component indicates once again that the inner refined magnetite is also a result of the first nucleated magnetite grains (pro-eutectoid product) and not only a product of oxide scale detachment and inner re-oxidation [37].

Therefore, the phase transformation within the oxide scale during hot rolling and subsequent cooling can be another reason to obtain this texture evolution [38, 39]. Some of these investigations

are underway to further understand how texture and grain size relate in oxide scales during steel processing at high temperatures.

4. Conclusions

The EBSD technique has been used to quantitatively evaluate the evolution of crystallographic orientations in the four ranges of individual grain sizes in the tertiary oxide scale of magnetite formed on hot-rolled steel. The following conclusions can be drawn.

(1) Phase identification and orientation mapping demonstrate that the {001} planes of magnetite and the {0001} planes of hematite are parallel to the oxide growth direction.

(2) The grain-refined magnetite near the oxide/substrate interface is thought to be a result of a pro-eutectoid reaction during hot rolling and cooling and re-oxidation during air-cooling after deformation. The refined magnetite grains surrounding the abnormal ones develop a strong texture component {001} parallel to the oxide growth.

(3) Ferrite grains in the steel substrate have the weak texture strength of 4.09. Magnetite samples with grain sizes of 1-5 μm and 5-10 μm have similarly strong texture strengths of 5.02 and 5.06. Pole figures representing discrete data allow a direct correlation of orientation and site in the large magnetite grains.

(4) ODFs indicate that magnetite develops the strong rotated cube texture component and that it shifts to the {100}<210> component. In contrast, magnetite with the grain size of 1-5 μm retains the {001}<100> cube texture component. The findings indicate that the formation mechanism of the

refined magnetite grains can be derived from the {001} fibre of magnetite re-oxidation during the recovery process after deformation, and the {110} fibre texture pro-eutectoid magnetite precipitated at high temperatures.

Acknowledgements

We are grateful to Mr. Joseph Abbott, Dr. Liang Hao and Mr. Stuart Rodd for their assistance in the HR-AC experiments. Special thanks are given to Dr. Azdiar Gazder and Dr. Mitchell Nancarrow for their support and vast sharing of experiences with regard to sample preparation and EBSD. The authors acknowledge the use of facilities within the UOW Electron Microscopy Centre.

References

[1] N. Birks, G.H. Meier, F.S. Pettit, Introduction to the High Temperature Oxidation of Metals, second ed., Cambridge University Press, New York, 2006.

[2] R. Bhattacharya, G. Jha, S. Kundu, R. Shankar, N. Gope, Surf. Coat. Technol. 201 (2006) 526–532.

[3] X.L. Yu, Z.Y. Jiang, J.W. Zhao, D.B. Wei, C.L. Zhou, Q.X. Huang, Effects of grain boundaries in oxide scale on tribological properties of nanoparticles lubrication, Wear, in press.

[4] D.J. Young, High Temperature Oxidation and Corrosion of Metals, Elsevier, Oxford, 2008.

[5] X.W. Cheng, Z.Y. Jiang, D.B. Wei, J.W. Zhao, B.J. Monaghan, R.J. Longbottom, L.Z. Jiang, Surf. Coat. Technol. 258 (2014) 257–267.

[6] D.H. Buckley, Prog. Surf. Sci. 12 (1982) 1–153.

[7] X.L. Yu, Z.Y. Jiang, D.B. Wei, C.L. Zhou, Q.X. Huang, D.J. Yang, Wear 302 (2013) 1286–1294.

[8] R.Y. Chen, W.Y.D. Yuen, Oxid. Met. 59 (2003) 433–468.

[9] M. Krzyzanowski, J.H. Beynon, D.C. Farrugia, Oxide Scale Behavior in High Temperature Metal Processing, Wiley-VCH, Weinheim, 2010.

[10] X.L. Yu, Z.Y. Jiang, J.W. Zhao, D.B. Wei, C.L. Zhou, Q.X. Huang, Corros. Sci. 85 (2014) 115–125.

[11] B. Gleeson, S.M.M. Hadavi, D.J. Young, Mater. High. Temp. 17 (2000) 311–319.

[12] B. Schmid, N. Aas, Ø. Grong, R. Ødegård, Oxid. Met. 57 (2002) 115–130.

[13] S. Hayashi, K. Mizumoto, S. Yoneda, Y. Kondo, H. Tanei, S. Ukai, Oxid. Met. 81 (2014) 357–371.

[14] R. Y. Chen, W. Y. D. Yuen, ISIJ Int. 45 (2005), 52–59.

[15] O. Engler, V. Randle, Introduction to Texture Analysis: Macrotexture, Microtexture, and Orientation Mapping, second ed., CRC press, Boca Raton, 2010.

[16] S.I. Wright, M.M. Nowell, R. de Kloe, P. Camus, T. Rampton, Ultramicroscopy 148 (2015) 132–145.

[17] P.J. Apps, J.R. Bowen, P.B. Prangnell, Acta Mater. 51 (2003) 2811–2822.

[18] X.L. Yu, Z.Y. Jiang, J.W. Zhao, D.B. Wei, C.L. Zhou, Q.X. Huang, Corros. Sci. 90 (2015) 140–152.

[19] X.L. Yu, Z.Y. Jiang, J.W. Zhao, D.B. Wei, C.L. Zhou, Q.X. Huang, ISIJ Int. 55 (2015) 278–284.

[20] Z.Y. Jiang, X.L. Yu, J.W. Zhao, C.L. Zhou, Q.X. Huang, G.Z. Luo, K.Z. Linghu, Adv. Mater. Res. 1017 (2014) 435–440.

[21] X.L. Yu, Z.Y. Jiang, J.W. Zhao, D.B. Wei, C.L. Zhou, Appl. Mech. Mater. 395 (2013) 273–278.

[22] X.L. Yu, Z.Y. Jiang, X.D. Wang, D.B. Wei, Q. Yang, Adv. Mater. Res. 415 (2012) 853–858.

[23] H.-J. Bunge, Texture Analysis in Materials Science: Mathematical Methods, Butterworth, Berlin, 1982.

[24] B.K. Kim, J.A. Szpunar, Orientation imaging microscopy in research on high temperature

oxidation, in: A.J. Schwartz (Ed.), Electron Backscatter Diffraction in Materials Science, Springer, New York, 2009, pp. 361–393.

[25] S. Birosca, D. Dingley, R.L. Higginson, J. Microsc. 213 (2004) 235–240.

[26] L. Suárez, P. Rodríguez-Calvillo, Y. Houbaert, N.F. Garza-Montes-de-Oca, R. Colás, Oxid. Met. 75 (2011) 281–295.

[27] L. Sun, K. Muszka, B.P. Wynne, E.J. Palmiere, Acta Mater. 66 (201) 132–149.

[28] J. Hu, L.X. Du, J.J. Wang, Q.Y. Sun, Mater. Des. 53 (2014) 332–337.

[29] P.G. Xu, F.X. Yin, Y.H. Huan, Y. Tomota, K. Nagai, Mater. Sci. Eng. A 433 (2006) 8–17.

[30] R. Song, D. Ponge, D. Raabe, R. Kaspar, Acta Mater. 53 (2005) 845–858.

[31] M. Kamaya, A.J. Wilkinson, J.M. Titchmarsh, Acta Mater. 54 (2006) 539–548.

[32] K. Shinoda, M. Demura, H. Murakami, S. Kuroda, S. Sampath, Surf. Coat. Technol. 204 (2010) 3614–3618.

[33] C. Juricic, H. Pinto, D. Cardinali, M. Klaus, C. Genzel, A.R. Pyzalla, Oxid. Met. 73 (2010) 15–41.

[34] A.A. Saleh, E.V. Pereloma, A.A. Gazder, Acta Mater. 61 (2013) 2671–2691.

[35] E.M. Lehockey, A.M. Brennenstuhl, I. Thompson, Corros. Sci. 46 (2004) 2383–2404.

[36] J. Paidassi, Acta Metall. 6 (1958) 184–194.

[37] A. Atkinson, Rev. Mod. Phys. 57 (1985) 437–470.

[38] W.J. Cheng, Y.Y. Chang, C.J. Wang, Surf. Coat. Technol. 203 (2008) 401–406.

[39] S. Valette, G. Trolliard, A. Denoirjean, P. Lefort, Solid State Ionics 178 (2007) 429–437.

List of figure and table captions

Fig. 1 EBSD (a) phase and (b) inverse pole figure (IPF) orientation maps of tertiary oxide scales formed on the steel substrate.

Fig. 2 EBSD (a) phase and (b) IPF orientation maps of the oxide scale with a grain size of 1-5 μm.

Fig. 3 EBSD (a) phase and (b) IPF orientation maps of the oxide scale with a grain size of 5-10 μm.

Fig. 4 EBSD (a) phase and (b) IPF orientation maps of the oxide scale with a grain size of 10-15 μm.

Fig. 5 EBSD (a) phase and (b) IPF orientation maps of the oxide scale with a grain size larger than 15 μm.

Fig. 6 Contoured (100) and (110) pole figures for (a) ferrite, (b) magnetite of the oxide scale with a grain size of 1-5 μm, and (c) magnetite with a grain size of 5-10 μm.

Fig. 7 Pole figures as scatter plots in the IPF colour scheme for magnetite with a grain size of (a) 10-15 μm, and (b) larger than 15 μm.

Fig. 8 Schematic representation of the position of the ideal fibres and some important texture components in cubic metals and alloys.

Fig. 9 Evolution of the crystallographic texture for magnetite in ODFs ϕ_2=0º and 45º sections for the (a) complete map, (b) grain size of 1-5 μm, and (c) grain size of 5-10 μm.

Fig. 10 Development of the texture intensity $f(g)$ along (a) θ and (b) the <110> fibres of magnetite with different ranges of grain sizes.

Table 1 Euler angles and Miller indices for some common texture components in cubic metals and alloys.

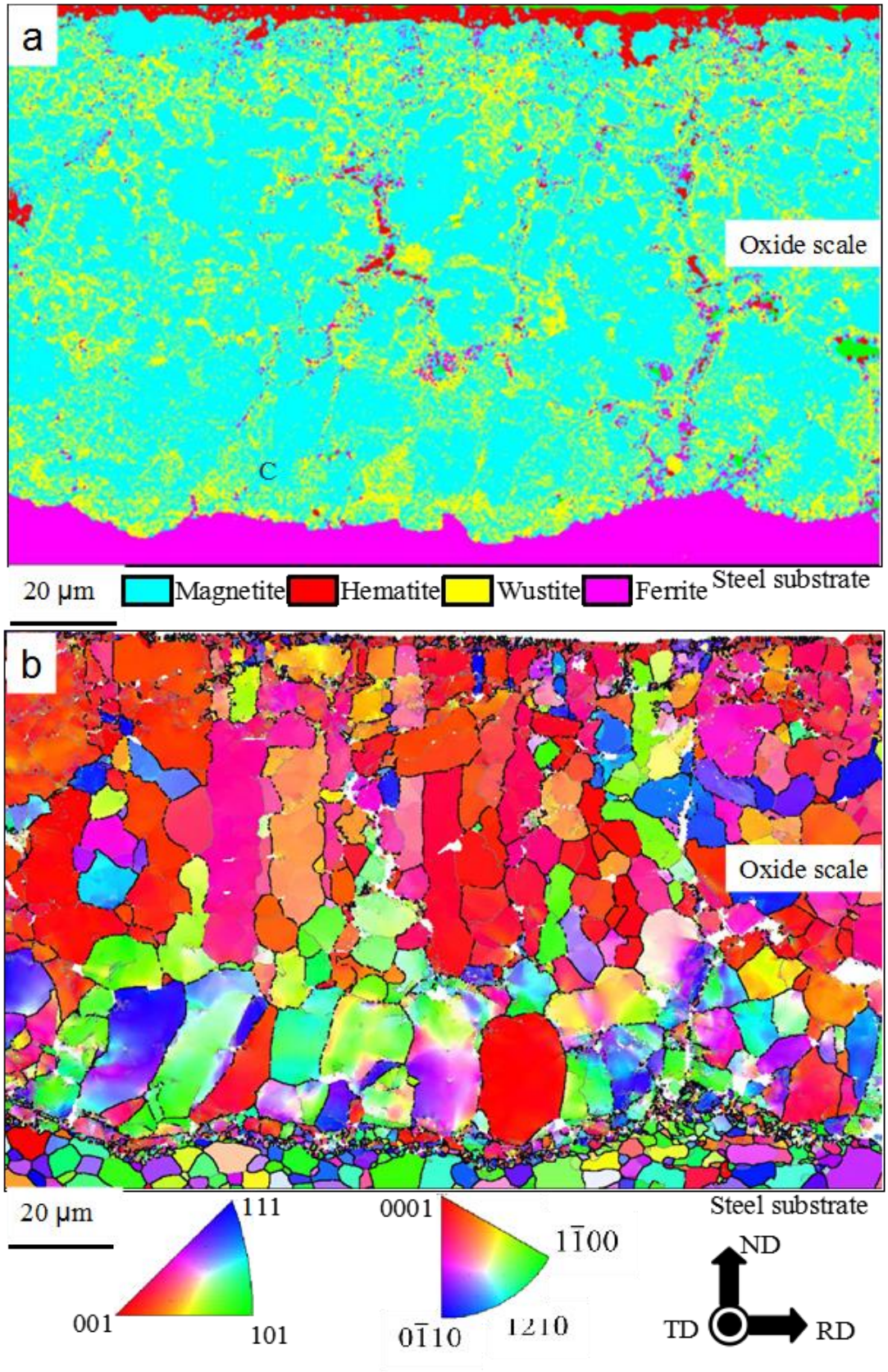

Fig. 1 EBSD (a) phase and (b) inverse pole figure (IPF) orientation maps of tertiary oxide scales formed on the steel substrate.

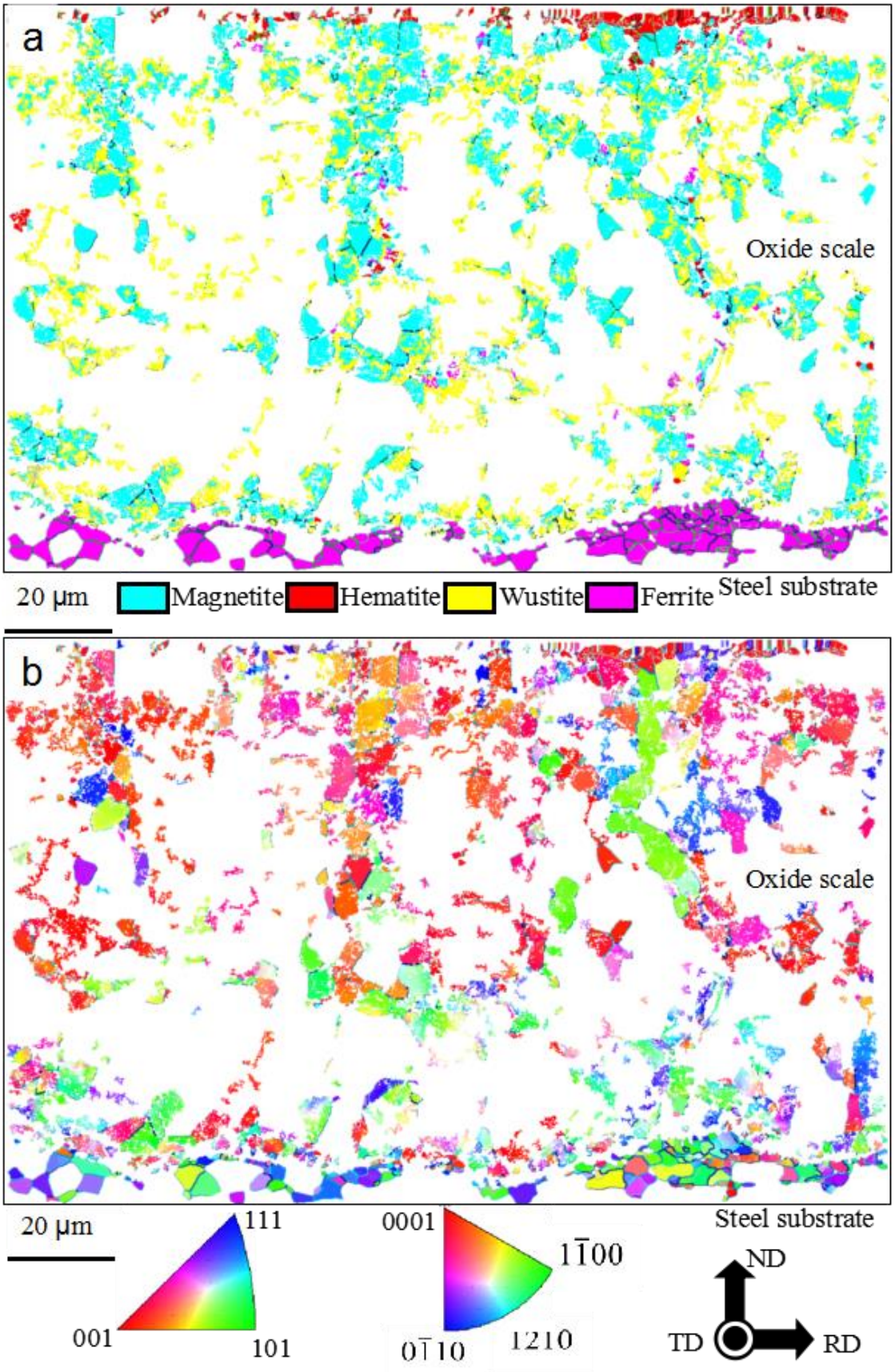

Fig. 2 EBSD (a) phase and (b) IPF orientation maps of the oxide scale with a grain size of 1-5 μm.

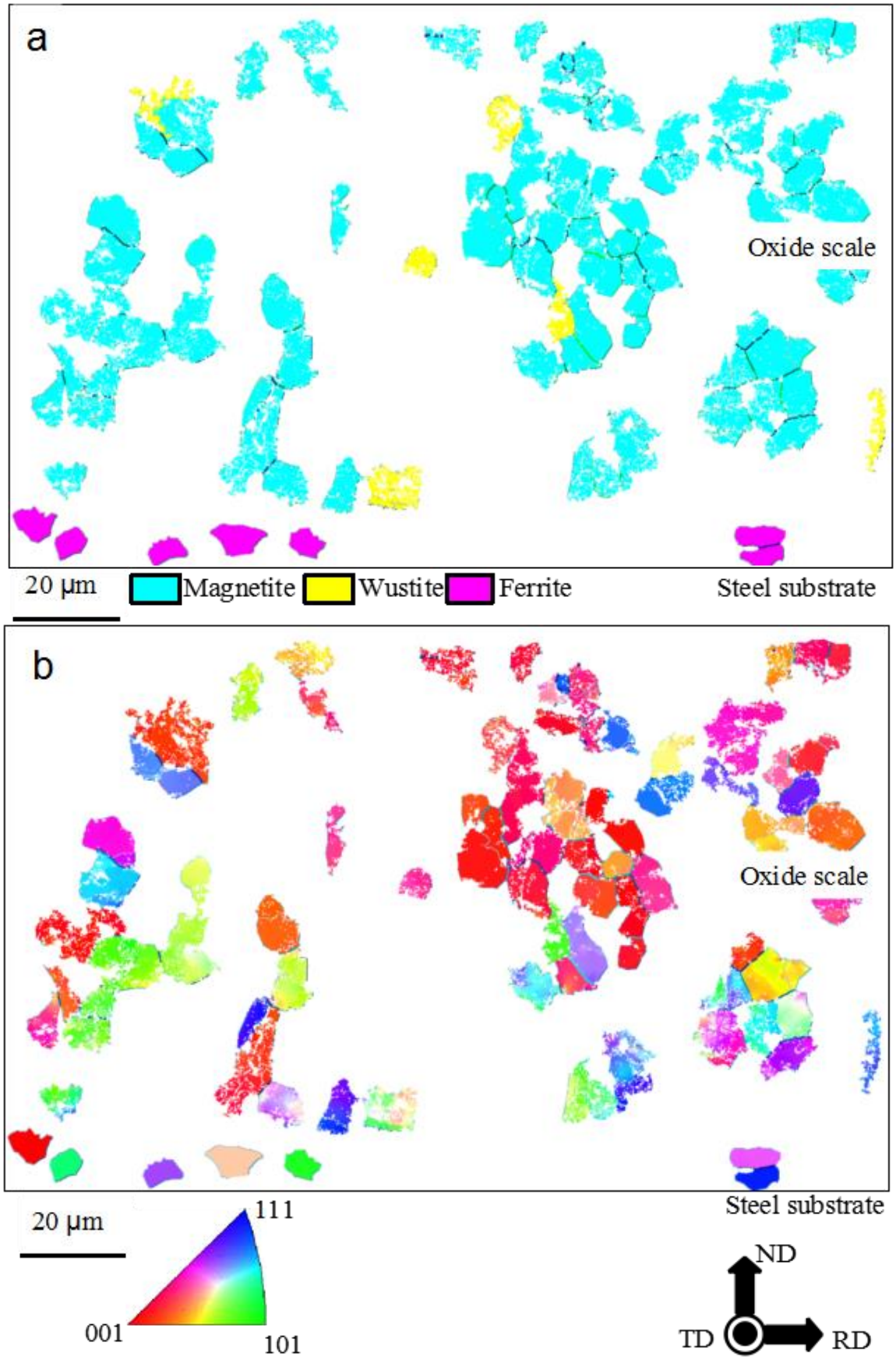

Fig. 3 EBSD (a) phase and (b) IPF orientation maps of the oxide scale with a grain size of 5-10 µm.

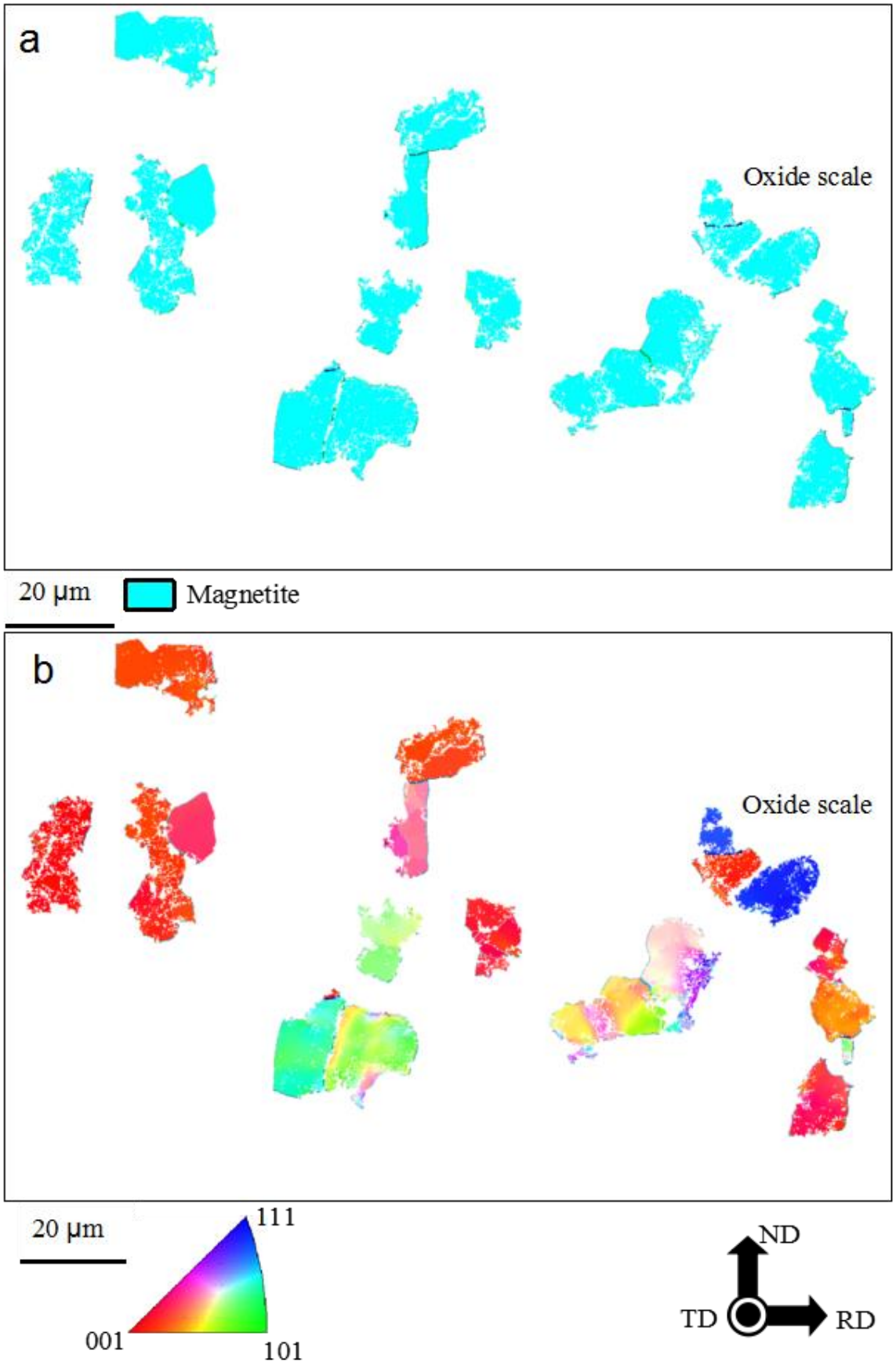
a
Oxide scale
20 µm
Magnetite
b
Oxide scale
20 µm
111
001
101
ND
TD
RD

Fig. 4 EBSD (a) phase and (b) IPF orientation maps of the oxide scale with a grain size of 10-15 μm.

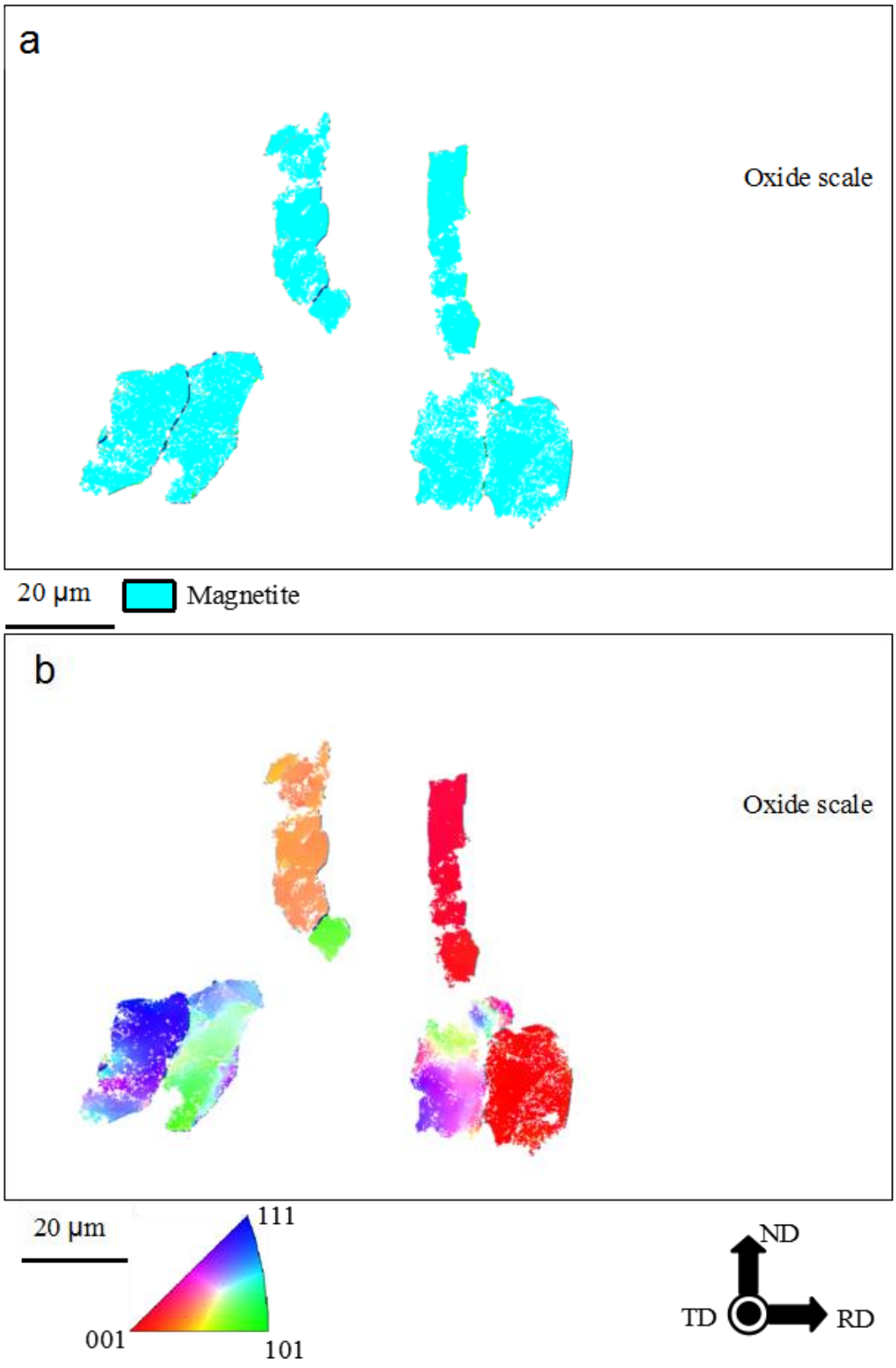

Fig. 5 EBSD (a) phase and (b) IPF orientation maps of the oxide scale with a grain size larger than 15 μm.

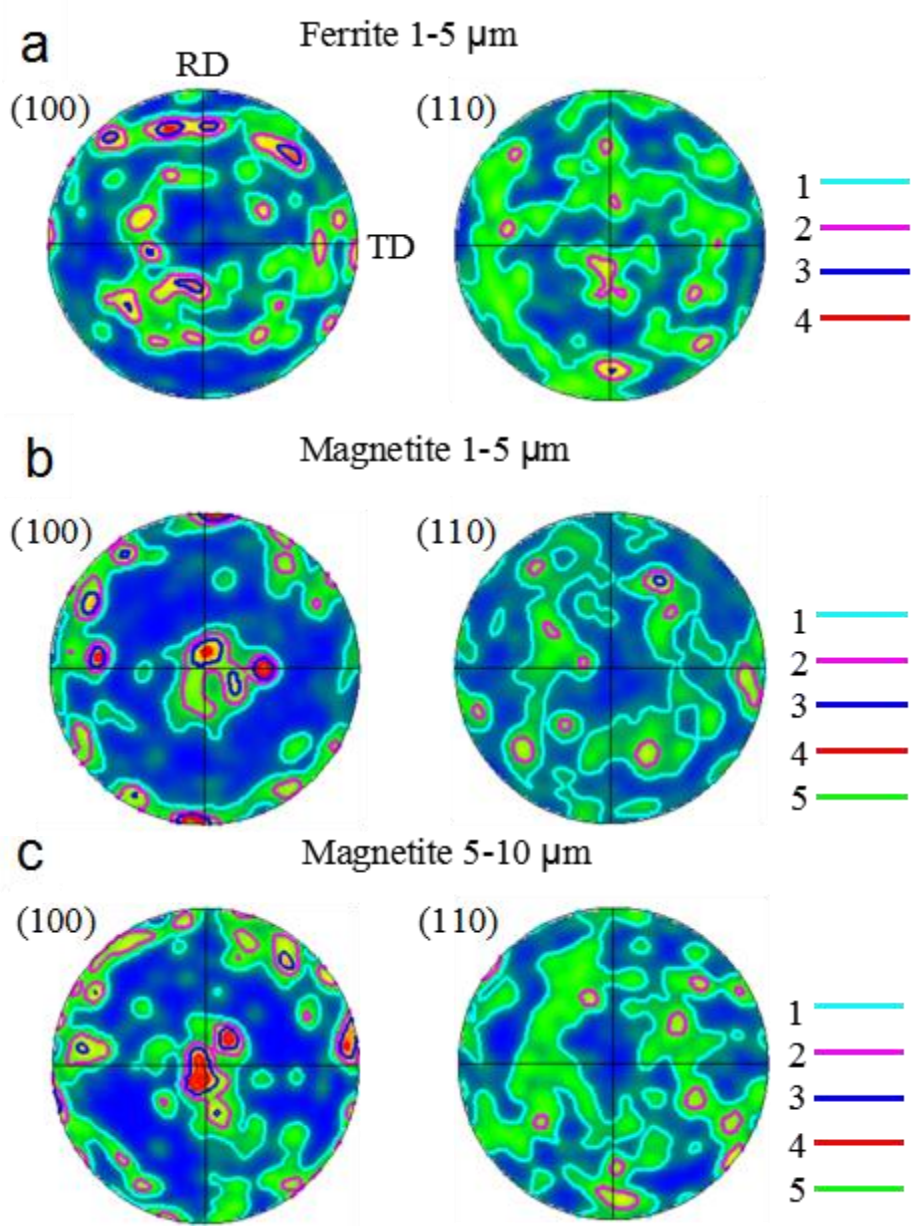

Fig. 6 Contoured (100) and (110) pole figures for (a) ferrite, (b) magnetite of the oxide scale with a grain size of 1-5 μm, and (c) magnetite with a grain size of 5-10 μm.

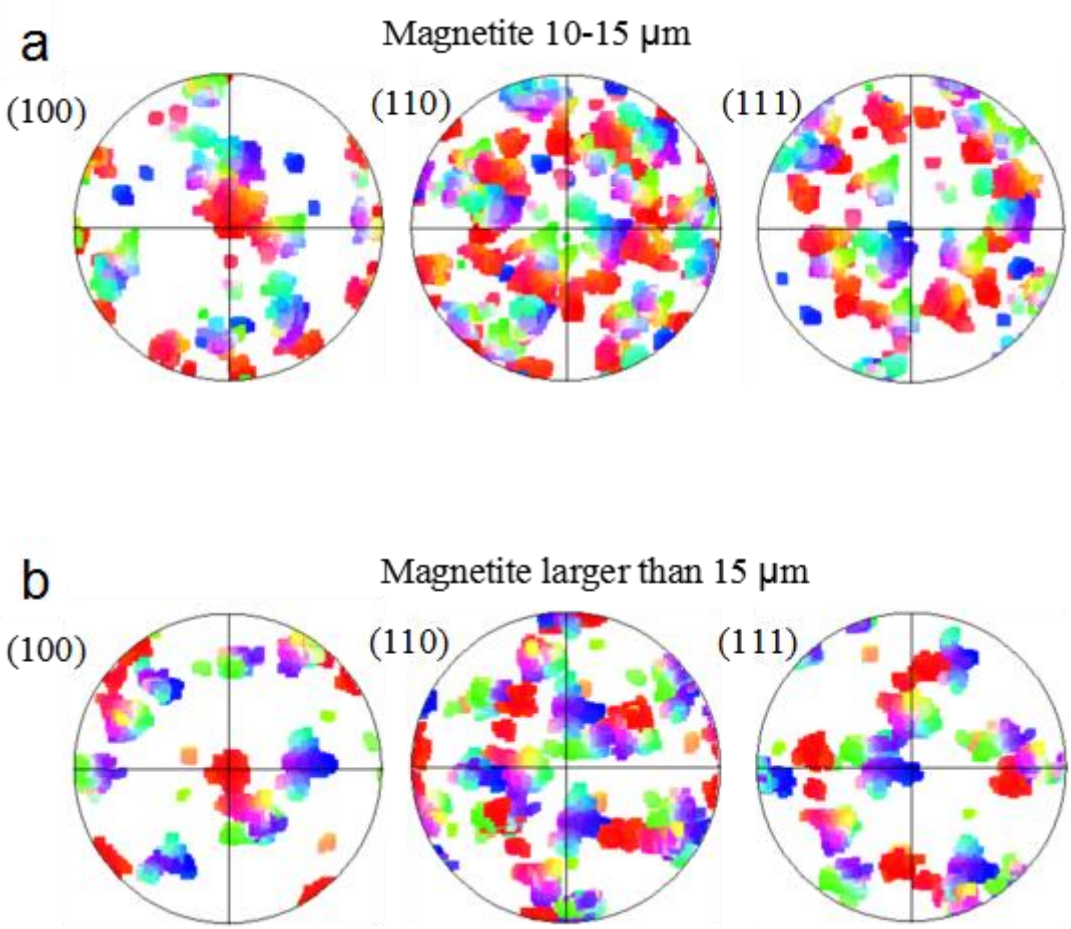

Fig. 7 Pole figures as scatter plots in the IPF colour scheme for magnetite with a grain size of (a) 10-15 µm, and (b) larger than 15 µm.

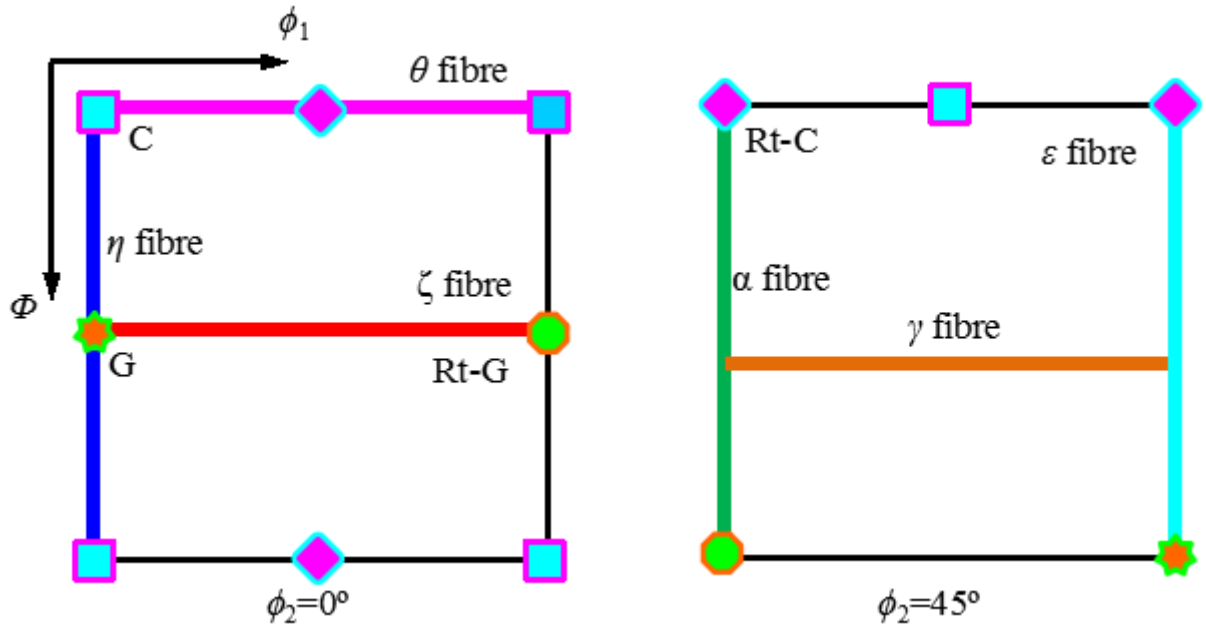

Fig. 8 Schematic representation of the position of the ideal fibres and some important texture components in cubic metals and alloys.

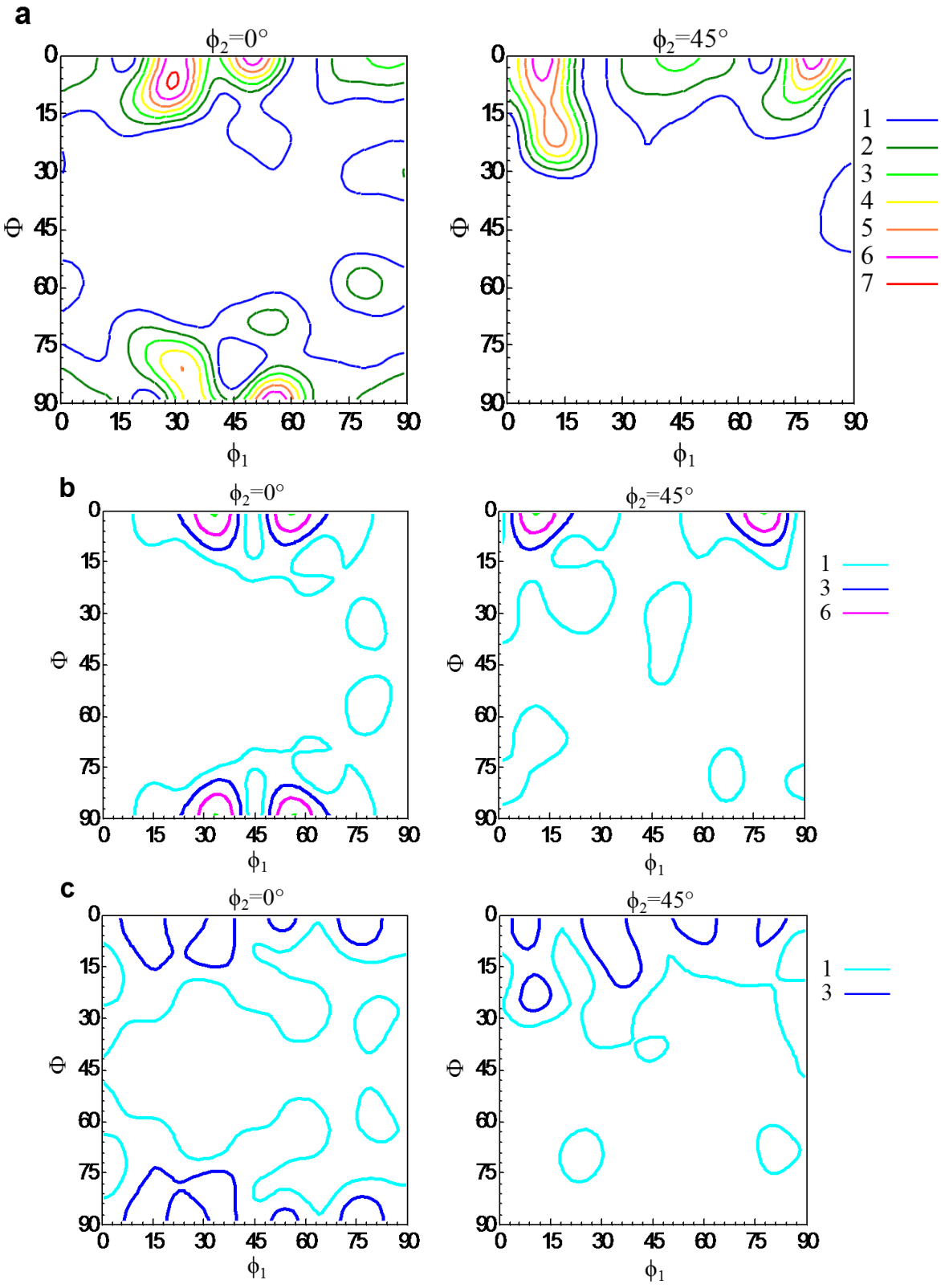

Fig. 9 Evolution of the crystallographic texture for magnetite in ODF ϕ_2=0º and 45º sections for the (a) complete map, (b) grain size of 1-5 μm, and (c) grain size of 5-10 μm.

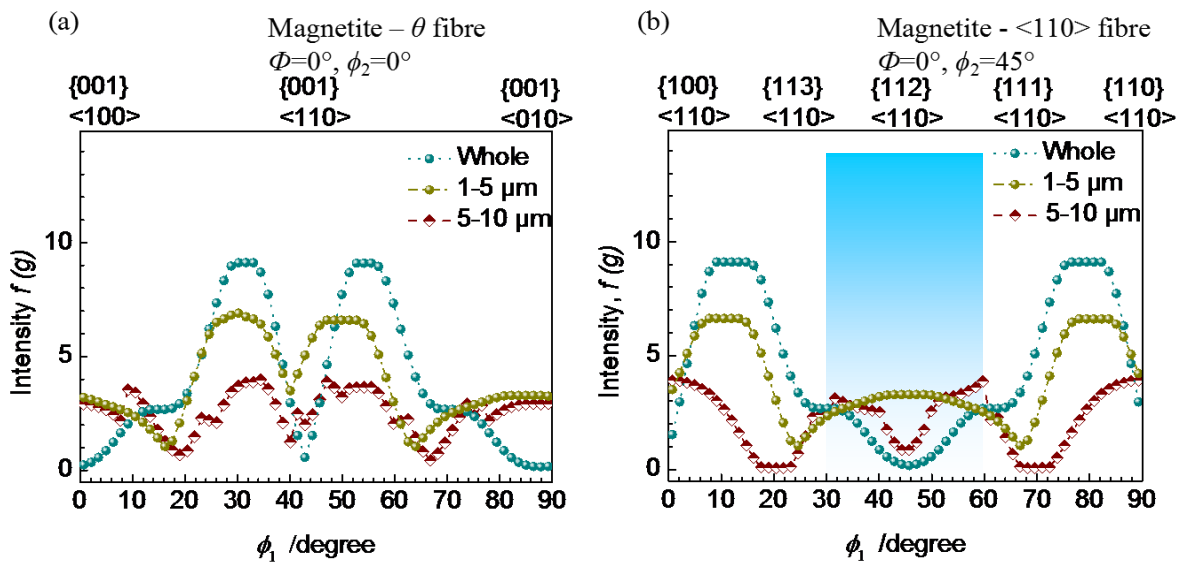

Fig. 10 Development of the texture intensity *f*(*g*) along the (a) θ and (b) the <110> fibres of magnetite with different ranges of grain sizes.

Table 1 Euler angles and Miller indices for some common texture components in cubic metals and alloys.

Texture component	Symbol	Euler angles			Miller indices	Fibre
		ϕ_1	Φ	ϕ_2		
Cube (C)		45	0	45	{001}<100>	<100>
Goss (G)		90	90	45	{110}<001>	<100>
Rotated Goss (Rt-G)		0	90	45	{011}<011>	<110>
Rotated Cube (Rt-C)		0/90	0	45	{001}<110>	<110>